(Received 12 May 2025, Accepted 18 July 2025, Scheduled 4 August 2025)

# Twelve-Element MIMO Antenna System Using Open-Slots for 5G Smartphones at Sub-6 GHz Band

Tanishk Thakur[1] and Naveen Jaglan[2,*]

[1] *Department of Electronics and Communication Engineering*
*Jaypee University of Information Technology, Waknaghat, Solan, Himachal Pradesh, India*
[2] *Centre of Excellence in 5G and IoT-Department of Electronics and Communication Engineering*
*Netaji Subhas University of Technology (NSUT), New Delhi, India*

**ABSTRACT:** This research offers a 12-element antenna array optimized for MIMO utilization in fifth-generation (5G) mobile phones. The antennas operate in the sub-6 GHz long-term evolution (LTE) frequency range, specifically between 3.4 and 3.6 GHz. To fulfil the growing demand for faster data speeds and reliable connection in 5G networks, the presented MIMO antenna setup offers a balance between compact size and high performance, making it well suited for integration into smartphones. Every radiating element in the array is tuned to approximately 3.5 GHz and features an open-slot structure, which effectively reduces mutual coupling and enhances isolation. Antenna arrangement has been constructed on an FR-4 substrate of dimensions 150 mm $\times$ 80 mm $\times$ 0.8 mm, corresponding to the layout restrictions of standard 6-inches smartphones. A prototype was developed to validate the design through measurements. The results demonstrate excellent impedance matching (return loss $>$ 10 dB), high isolation ($>$ 20 dB), strong radiation efficiency (exceeding 66%), and a low envelope correlation coefficient ($<$ 0.03) covering the target frequency range.

## 1. INTRODUCTION

The design specifications for mobile devices, notably smartphones, have changed significantly as a result of fast-paced progress in wireless communication technology, especially with the introduction of 5G. Antennas that can meet these cutting-edge communication requirements are becoming more and more in demand as 5G networks strive to come up with extremely fast data transfer rates, low latency, and high dependability. Multi-input multi-output (MIMO) framework becomes a viable option among the several antenna designs for enhancing network performance and data throughput. The sub-6 GHz frequency spectrum is necessary to 5G cell phone applications because it strikes a balance among coverage, data rate, and propagation characteristics. The design of effective, small, and high-performance MIMO antenna systems becomes crucial to satisfying the increasing need for dependable and fast communication in this range. However, integrating many antennas while preserving optimal performance is extremely difficult due to the small amount of space available in smartphones. The vast MIMO improves spectral efficiency and channel capacity for 5G mobile communication compared to low-order techniques ($2 \times 2$ or $4 \times 4$ MIMO) used in 4G long-term-evolution frameworks [1, 2]. Effective array decoupling is necessary to stimulate diversity and multiplexing potentials at the moment, and 5G MIMO in the sub-6 GHz frequency range can tolerate isolation level of 10 dB. However, the bottom threshold of isolation needs to be raised to greater than 15 dB in order to improve MIMO performance. Mobile phone antennas are shrinking as customers prefer slim and lightweight handsets. This raises the level of complexity of antenna design requirements. The antenna element should be small, well decoupled, and suitably positioned on the phone's printed circuit board (PCB) or rim. Multiple antenna systems for 5G networks may enhance the spectrographic effectiveness and channel capacity; however, fitting multiple antennas into a smartphone's restricted size is hard. For optimal MIMO performance, the separation between antenna elements must exceed 15 dB [3]. Researchers around have proposed many approaches to increase isolation between antenna parts. There are numerous decoupling structures, such as extended ground plane [4], electromagnetic band gaps [5], parasitic components [6], T-shaped slots [7], and nullification lines [8]. One issue with some decoupling mechanisms is that they affect the entire antenna efficiencies. Researchers have proposed numerous approaches to improve isolation [9–12], including asymmetrical similar antennas [13, 14], and methods for designing self-isolated antennas [15] include orthogonal manner pairs [16] and isolating gap and shorting strip [17]. In [18], an eight-component MIMO system for LTE band 42 is presented that, even though it necessitates an adequate amount of space, achieves an estimated channel capacity about 16 bps/Hz at a signal-to-noise ratio of 20 dB. In [19], a ten antenna MIMO system is proposed to operate in LTE bands 42 and 43. The channel capacity at 20 dB SNR was calculated to be 47 bps/Hz. Ref. [20] proposes an $8 \times 8$ MIMO antenna system operating at frequency of 2.6 GHz with 20 dB SNR and an overall channel capacity of 40 bps/Hz. Designing the MIMO system without external decoupling can improve isolation without reducing efficiency. However, augmenting the antenna ar-

* Corresponding author: Naveen Jaglan (naveenjaglan1@gmail.com).

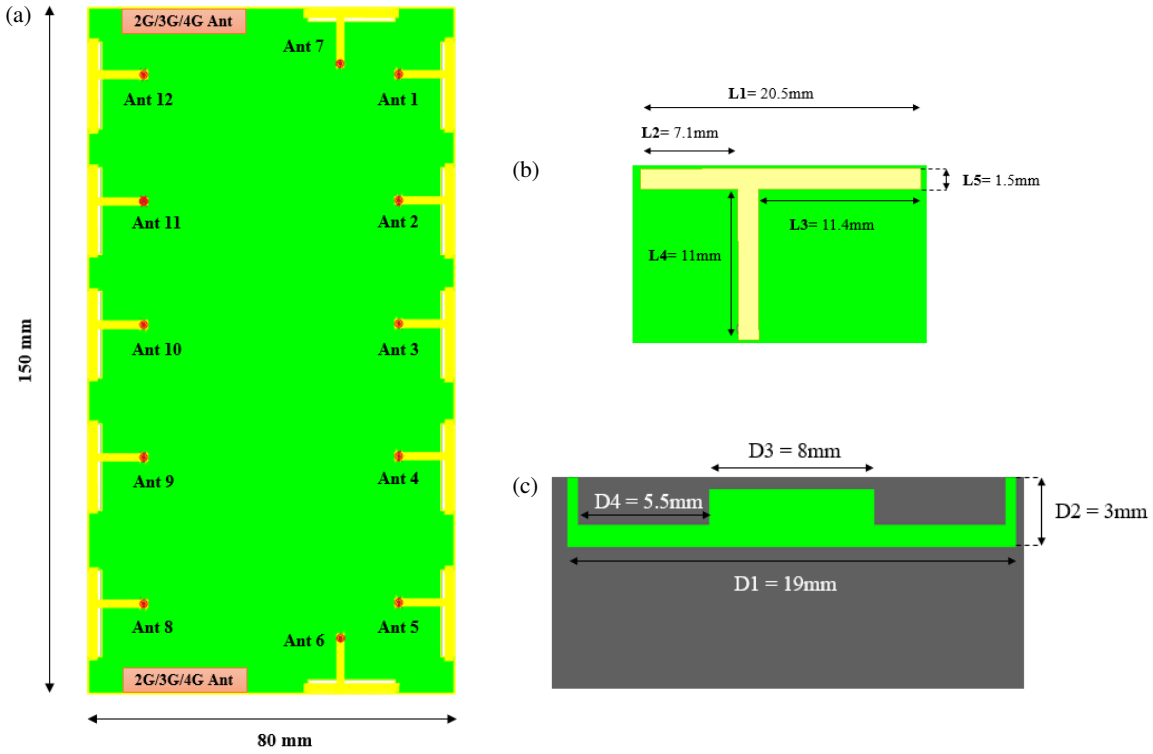


**FIGURE 1**. (a) Design of the intended 12-element MIMO antenna. (b) Design of T-shape antenna. (c) Open slot design in an E form.

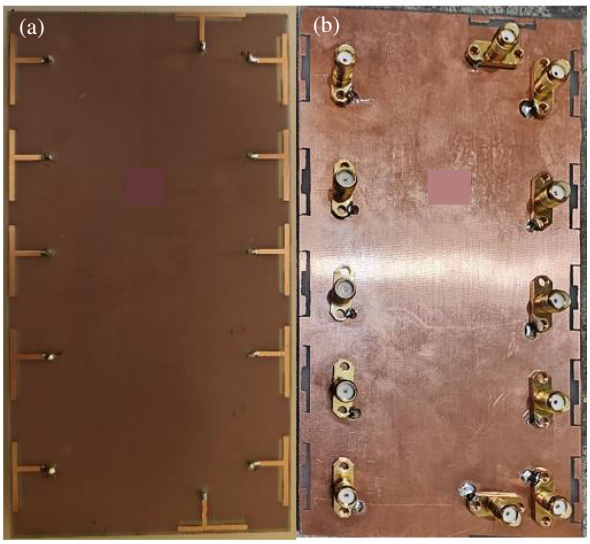


**FIGURE 2**. Fabricated antenna configurations. (a) Top view. (b) Bottom view.

ray size while maintaining appropriate isolation and efficiency is a challenge in improving ergodic channel capacity. In MIMO arrangements, antennas must be correctly field and port decoupled to ensure uncorrelated channels, including cavity for 2G/3G/4G antennas to ensure a controlled progression to the 5G communication system. This work proposes a 12-element MIMO architecture for the sub-6 GHz range. The T-shaped microstrip element powered with coaxial feed is developed for LTE band 42 (3.4–3.6 GHz). The antenna's independence from external decoupling structures results in excellent total efficiency. The ground plane features open ended slots to provide the isolation between separate antennas. The cross-coupling suppression among antenna elements exceeds 20 dB, resulting in a total efficiency of over 66%. The greatest ergodic channel capacity at 20 dB SNR is 65.8 bps/Hz. Open-ended slots in the conductive surface provide effective separation between antenna elements. All 12 elements are neatly positioned on the conducting plane, and there is space for 2G/3G/4G antennas. The presented architecture is simulated after it is fabricated and then tested. Figure 1(a) showcases the suggested arrangement for the MIMO system. The presented design consists of twelve antenna elements, labelled 1 to 12. The antenna elements are fabricated on an FR4 substrate with a relative permittivity of 4.4 and a loss tangent of 0.02, which is copper-coated on both sides.

## 2. PROPOSED MIMO ANTENNA DESIGN

The measurements of substrate are 150 mm × 80 mm × 0.8 mm and suitable for 6-inch 5G cell phones. This base material, commonly known as a printed circuit board (PCB), contains a yellow antenna feeding line on upper side and a conductive plane on the bottom in green tone. Ants 6 and 7 are arranged horizontally along the shorter edges, whereas Ants 1–5 and Ants 8–12 are put vertically over the longer edges. The white rectangular gap on the shorter edges is designed to accommodate 2G/3G/4G antennas. Figure 1(b) presents the structure of a single slot antenna element. The slot radiator consists of three sections: vertical open-end, horizontal slot, and branch slots. The two vertical open-end portions have the same length of 3 mm

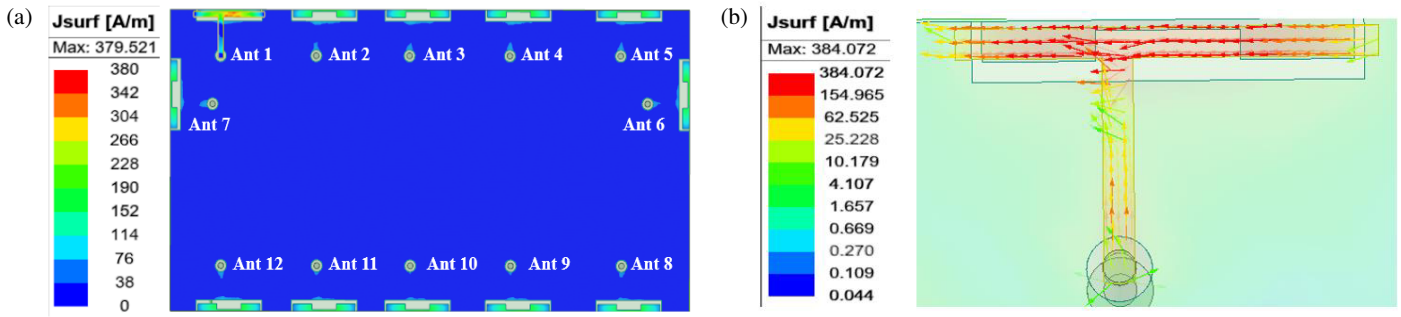


**FIGURE 3**. (a) Surface current spread on the ground plane at 3.5 GHz when Ant 1 is activated. (b) Vector surface current distribution.

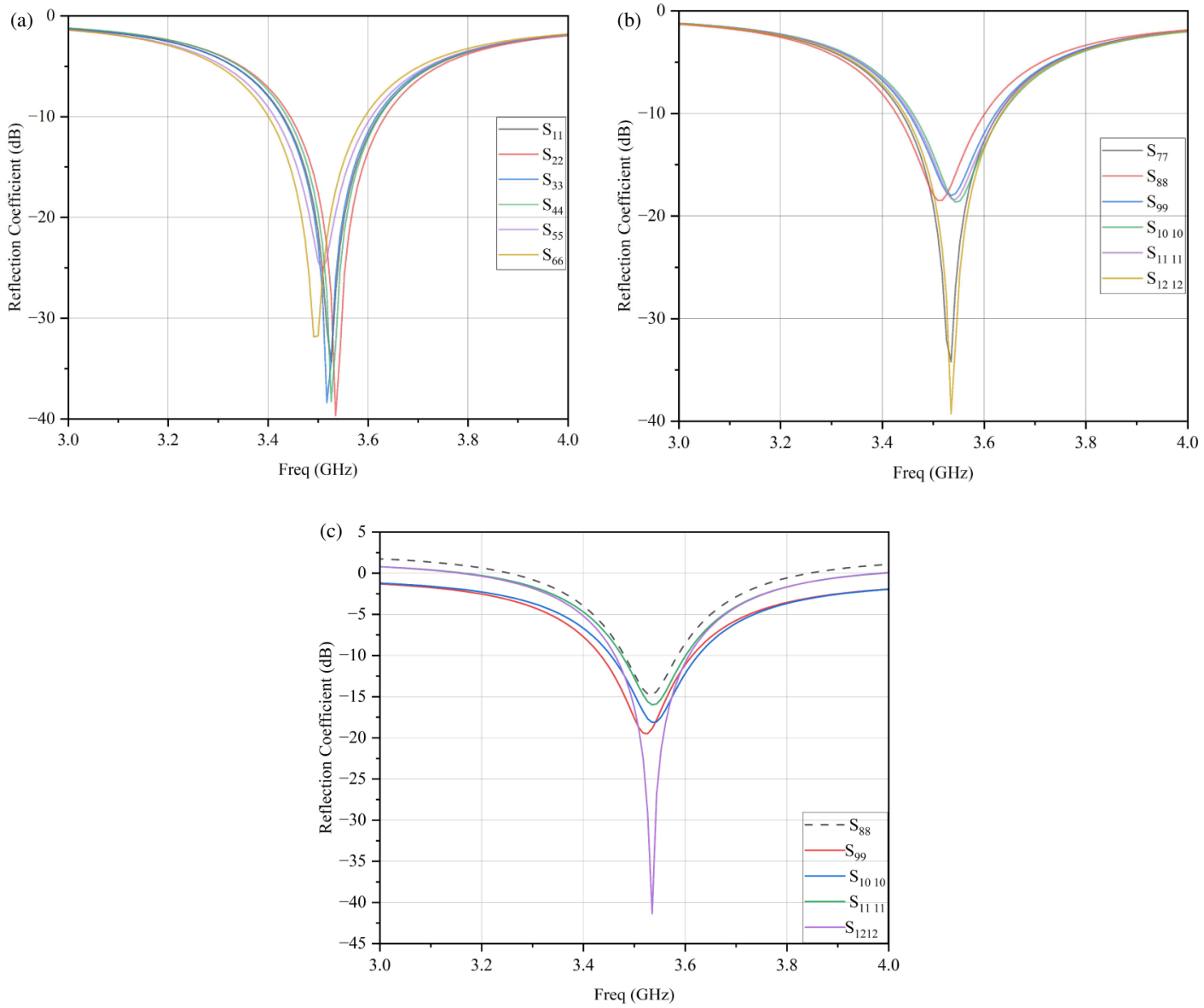


**FIGURE 4**. (a) Simulated reflection coefficient from Ant 1 to Ant 6. (b) Reflection coefficient from Ant 7 to Ant 12. (c) Measured Reflection Coefficient for Ant 7 to Ant 12.

and same width of 0.5 mm, respectively. Here, a T-shaped feeding line is used which offers optimal impedance matching and radiation efficiency values. The presented antenna element with an E-shaped open-end slot has the dimensions as follows: $L1 = 20.5$ mm, $L2 = 7.1$ mm, $L3 = 11.4$ mm, $L4 = 11$ mm, $L5 = 1.5$ mm. Similarly, the dimensional configuration for the open-ended E-shaped slot as shown in Figure 1(c) is as follows: $D1 = 19$ mm, $D2 = 3$ mm, $D3 = 8$ mm, and $D4 = 5.5$ mm.

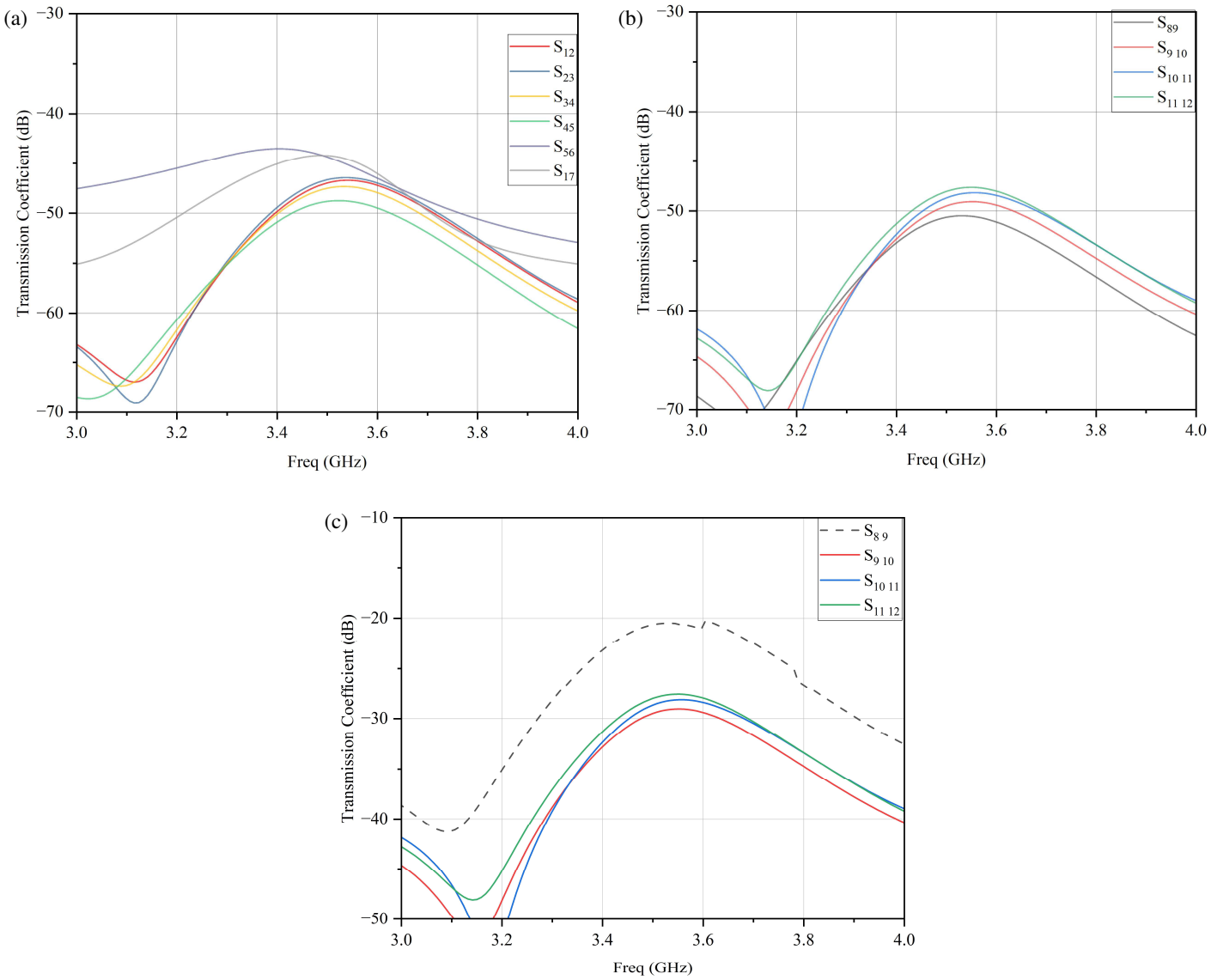


**FIGURE 5**. Here (a) and (b) show simulated mutual coupling between the various combinations of the antenna arrangements. (c) Measured mutual coupling between Ants 8 to 12.

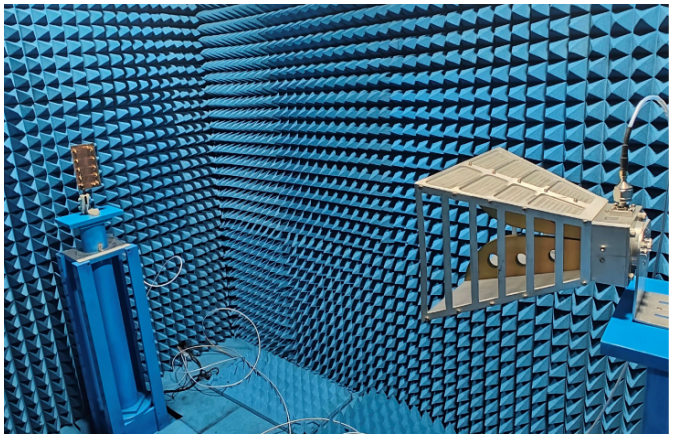

**FIGURE 6**. Presented antenna in an anechoic chamber for the testing.

The T-shaped 50-ohm microstrip line is constructed which is connected through the end point of $L4$. The effective length of T-shaped antenna is a combination of $\lambda/4$ and $\lambda/2$ resonant segments.

$$L_{eff} = L_{vert} + \frac{1}{2}L_{horiz} \tag{1}$$

where $L_{vert}$ is the vertical arm length, and $L_{horiz}$ is the horizontal arm length.

$$f_r = \frac{c}{4L_{eff}\sqrt{\varepsilon_{eff}}} \tag{2}$$

where $f_r$ is the resonant frequency, $c$ the speed of light, and $\varepsilon_{eff}$ the effective dielectric constant.

For the open-slot E-shaped structure, the resonant modes are determined by the slot lengths etched into the ground. Each arm

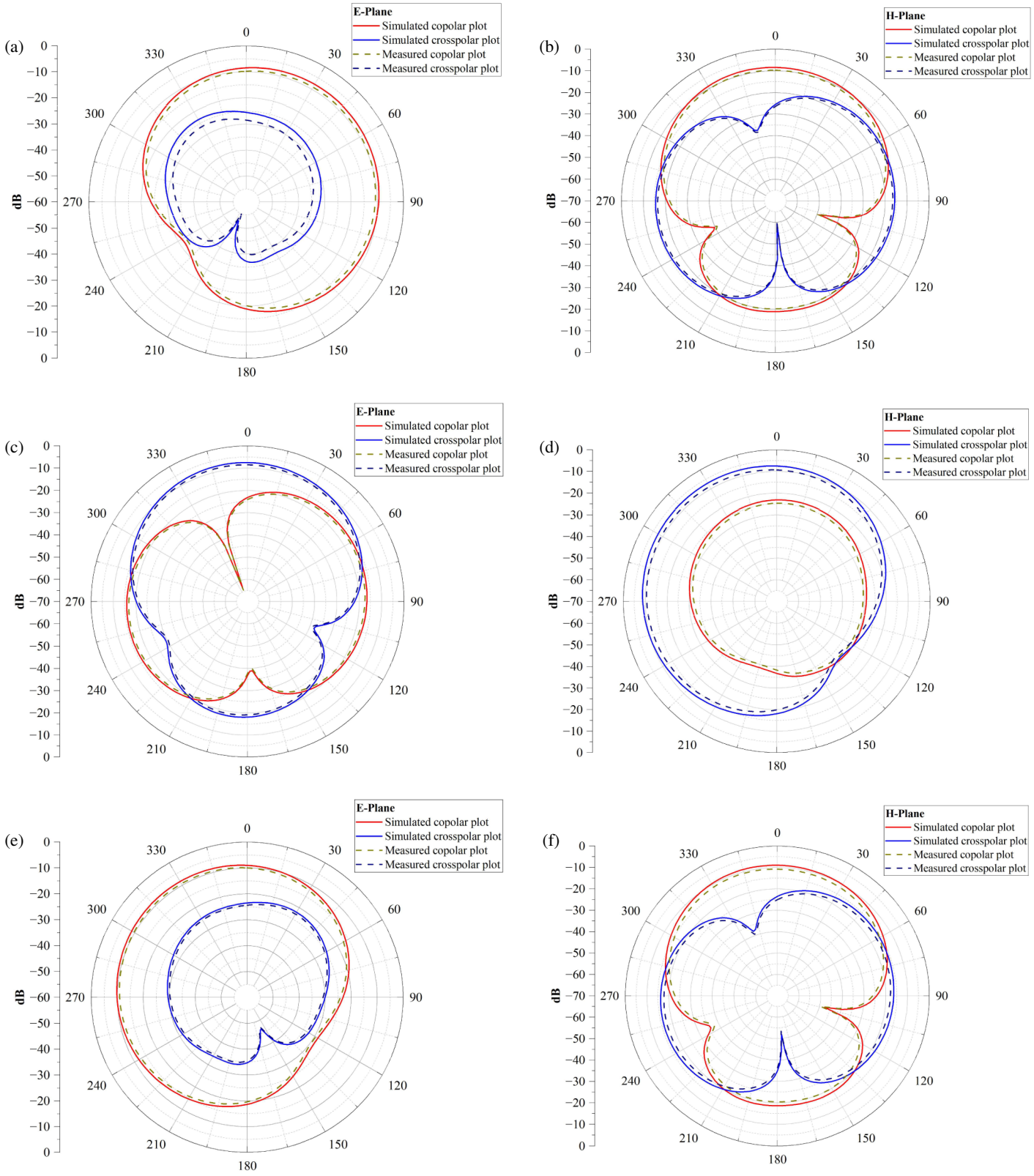


**FIGURE 7**. Radiation characteristics on $E$-plane and $H$-plane. (a) Ant 3 on $E$-plane, (b) Ant 3 on $H$-plane. (c) Ant 7 on $E$-plane. (d) Ant 7 on $H$-plane. (e) Ant 10 on $E$-plane. (f) Ant 10 on $H$-plane.

behaves as a resonant cavity, and the effective resonance is

$$f_r = \frac{c}{2L_{slot}\sqrt{\varepsilon_{eff}}} \tag{3}$$

where $L_{slot}$ is the total effective length of each slot arm. The proposed design has been fabricated. Figures 2(a) and 2(b) depict the top and bottom sides of a generated sample. The simu-

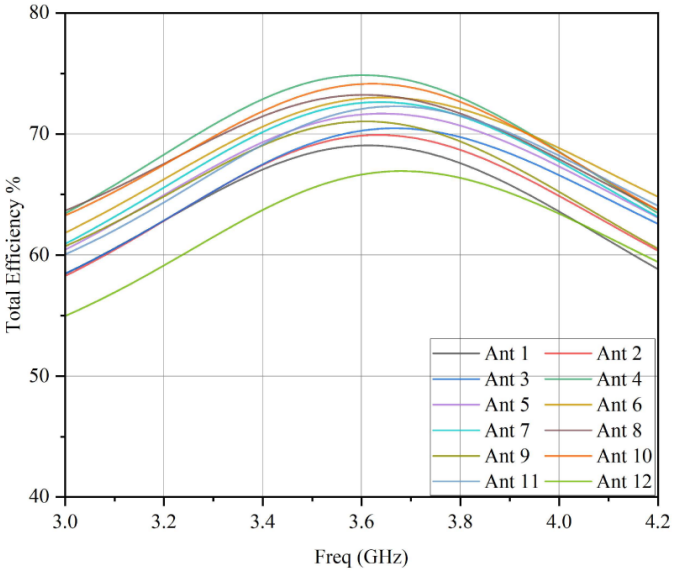


**FIGURE 8**. Simulated radiation efficiencies from Ant 1 to the Ant 12.

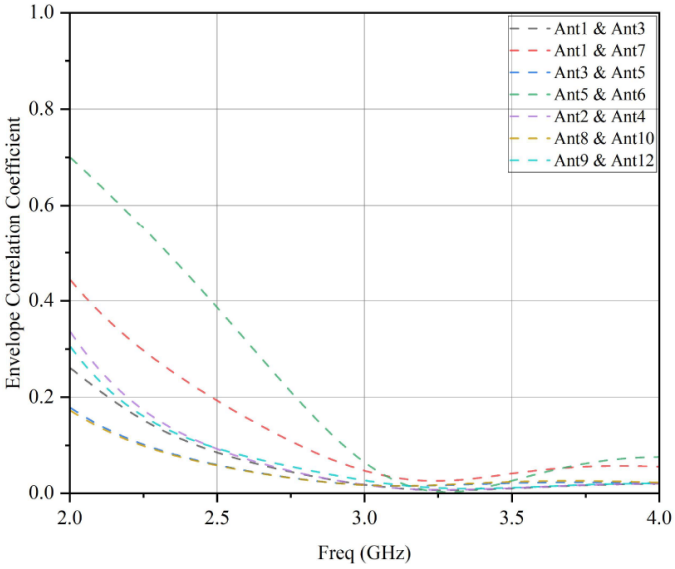


**FIGURE 9**. Envelope correlation coefficient (ECC) values were calculated for various antenna elements.

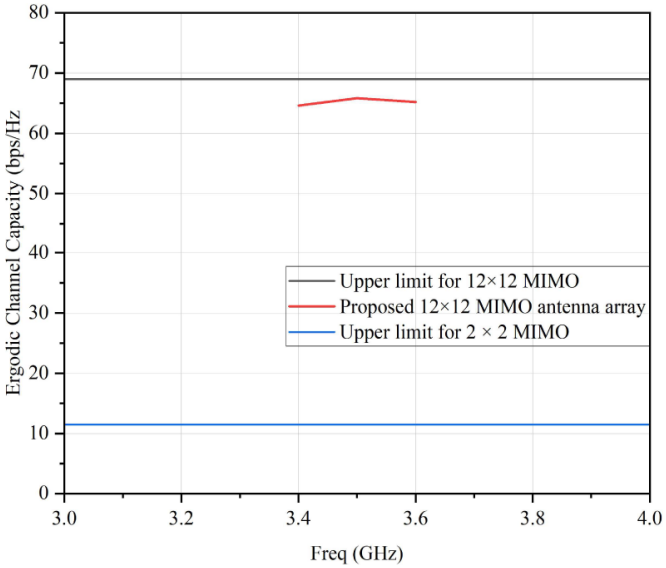


**FIGURE 10**. Ergodic channel capacity calculated using measured values.

lated current spread on the radiating element structure is illustrated in Figure 3. Specifically, Figure 3(a) presents that the current spreads are observed when Ant 1 is activated in isolation. As evident from the figure, when Ant 1 is activated, the surface current remains concentrated around its vicinity and does not significantly spread to adjacent elements or components of the antenna system. This localized current behaviour effectively minimizes the mutual coupling with nearby antenna elements, which is crucial for ensuring good isolation and maintaining optimal MIMO performance. Figure 3(a) further provides insight into the surface distribution of current on the ground plane of the suggested antenna arrangement. The analysis reveals that strong current flows are observed along shorter paths on the ground plane, particularly around regions where the slots are narrower. In contrast, the larger dimensions of the slot cause the surface currents to propagate in opposing directions, resulting in a reduction of current magnitude along those wider sections. Additionally, the electric field intensity tends to peak near the centre of the larger slot dimensions, highlighting regions of strong electromagnetic activity. The interaction between the electric field distribution inside the slot and the surrounding surface current paths plays a pivotal role in the overall radiation behaviour of the antenna.

## 3. RESULTS AND ANALYSIS

### 3.1. S-Parameters, Efficiency and Radiation Patterns

Figure 4(a) presents simulated outcomes of reflection coefficients for Ants 1–6. Figure 4(b) illustrates the simulated reflection parameters for Ants 7–12. The reflection coefficients for all antennas exceed 18 dB on LTE band 42. The suggested design uses identical antennas, resulting in similar reflection coefficient values. While measuring the reflection coefficient of just one element, the remaining antennas are closed off with 50 ohms. Figure 4(c) shows measured reflection coefficient values for Ants 7 to 12, validating the simulation results. Figures 5(a) and (b) illustrate the isolation of nearby antennas. The design delivers more than $-42.5$ dB of isolation between any two antennas. Figure 5(c) illustrates the measured mutual coupling between the antenna elements where $-20$ dB of isolation is achieved. The mutual coupling between antenna elements is analyzed primarily through surface, $S$-parameter behaviour (particularly $S_{12}$, $S_{23}$ etc.), and envelope correlation coefficient (ECC). Since $S_{12}$ quantifies the power transferred between ports, it inherently reflects isolation without need to introduce isolation loss. Here, antenna element has good impedance matching and placement, with no impact on neighbouring elements' reflection coefficients.

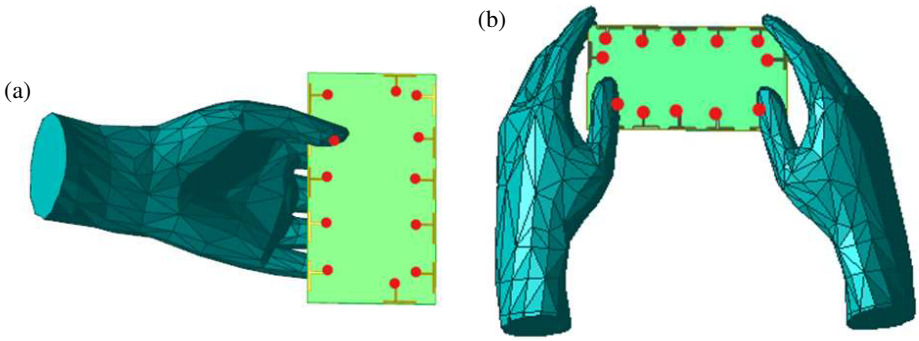


**FIGURE 11**. Representation of a portable mobile phone used in two different modes: (a) Single hand mode (SHM). (b) Dual hand mode (DHM).

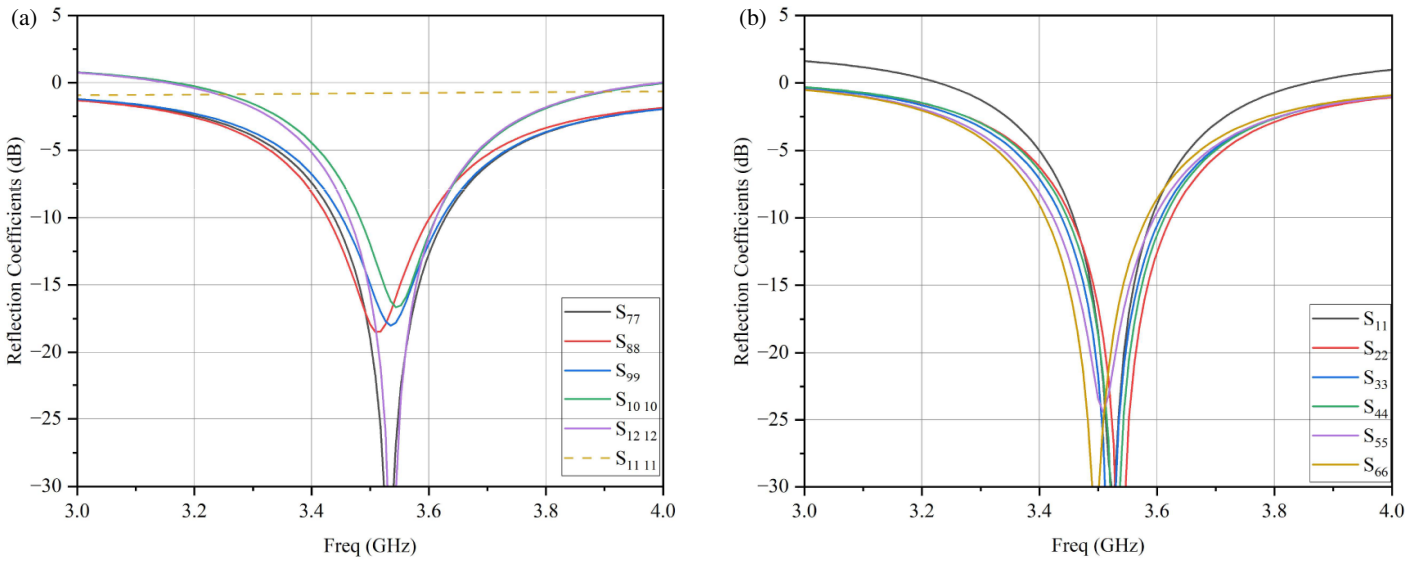


**FIGURE 12**. Simulated reflection coefficients considering SHM. (a) Ant 7 to Ant 12. (b) Ant 1 to Ant 6.

The prototype was fabricated using accurate PCB process that closely matched the design specifications slot shape feed points; trace dimensions were carefully maintained; and measurements were carried out in a calibrated anechoic chamber as shown in Figure 6 resulting in nearly identical results. In Figure 7, the radiation plot is shown, and as the proposed array's antennas have similar dimensions and are symmetrically positioned, only findings for Ants 3, 7, and 10 are displayed. Simulated and measured results on $E$-plane and $H$-plane are shown from Figure 7(a) to Figure 7(f). Here, Figure 8 displays the simulated antenna efficiency. Efficiency metrics are presented under unloaded conditions to represent best case radiative behaviour of the proposed system over 66%. Radiation efficiency values are within acceptable ranges for cellular communication [21].

### 3.2. The Diversity and the Multiplexing Parameters

This section evaluates critical MIMO antenna characteristics, including correlation coefficient and ergodic channel capacity. ECC determines the relationship between the radiation patterns generated by two radiators throughout every MIMO system. ECC value less than 0.5 is considered as high diversity outcomes for 5G MIMO systems [22]. When ECC exceeds 0.5, antenna elements and channel routes are highly correlated, resulting in poor MIMO antenna performance. MIMO systems require signal independence for optimal diversity and spatial multiplexing. Figure 9 highlights the correlation coefficient between the different combinations of the antenna elements. The ECC between different antenna elements is calculated as below 0.03.

$$ECC = \left| \frac{\int_0^{2\pi}\int_0^{\pi} \left(XPR \cdot E_{\theta i} \cdot E^*_{\theta j} \cdot P_\theta + XPR \cdot E_{\emptyset i} \cdot E^*_{\emptyset j} \cdot P_\emptyset\right) \sin(\theta)\, d\theta d\emptyset}{\sqrt{\prod_{k=i,j} \int_0^{2\pi}\int_0^{\pi} \left(XRP \cdot E_{\theta k} \cdot E^*_{\theta k} \cdot P_\theta + XRP \cdot E_{\emptyset k} \cdot E^*_{\emptyset k} \cdot P_\emptyset\right) \sin(\theta)\, d\theta d\emptyset}} \right|^2 \quad (4)$$

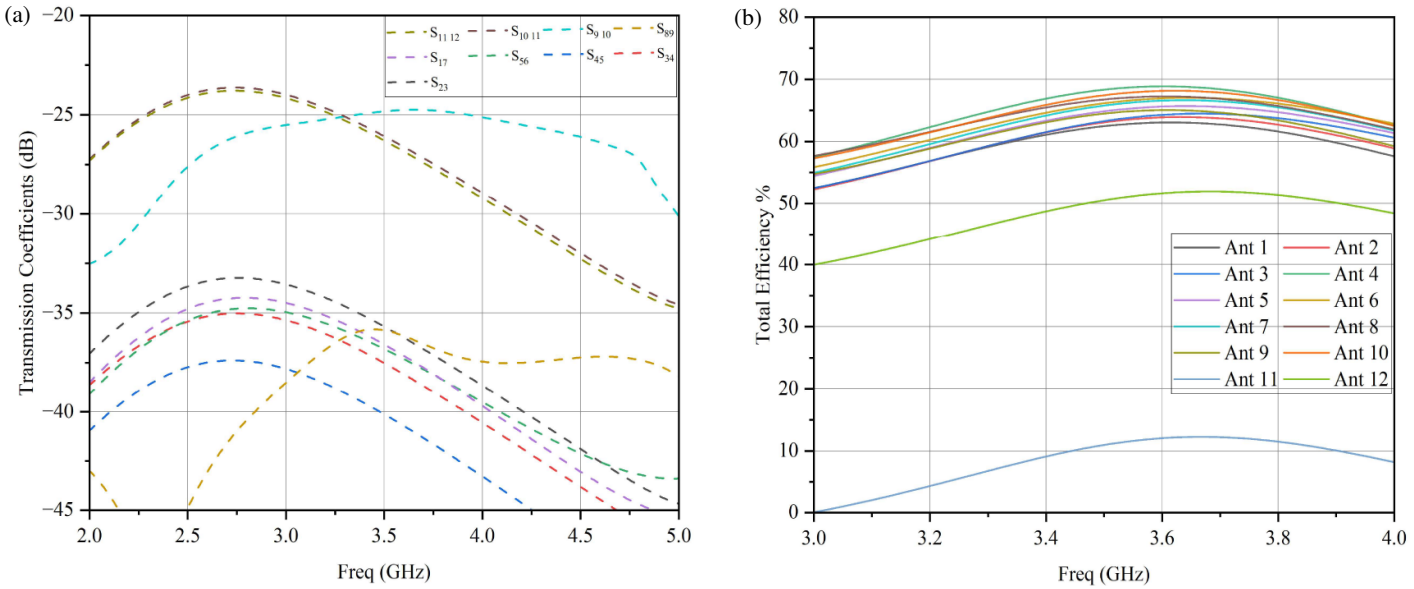


**FIGURE 13**. (a) Transmission coefficients of the antenna system for SHM. (b) Simulated efficiency for SHM.

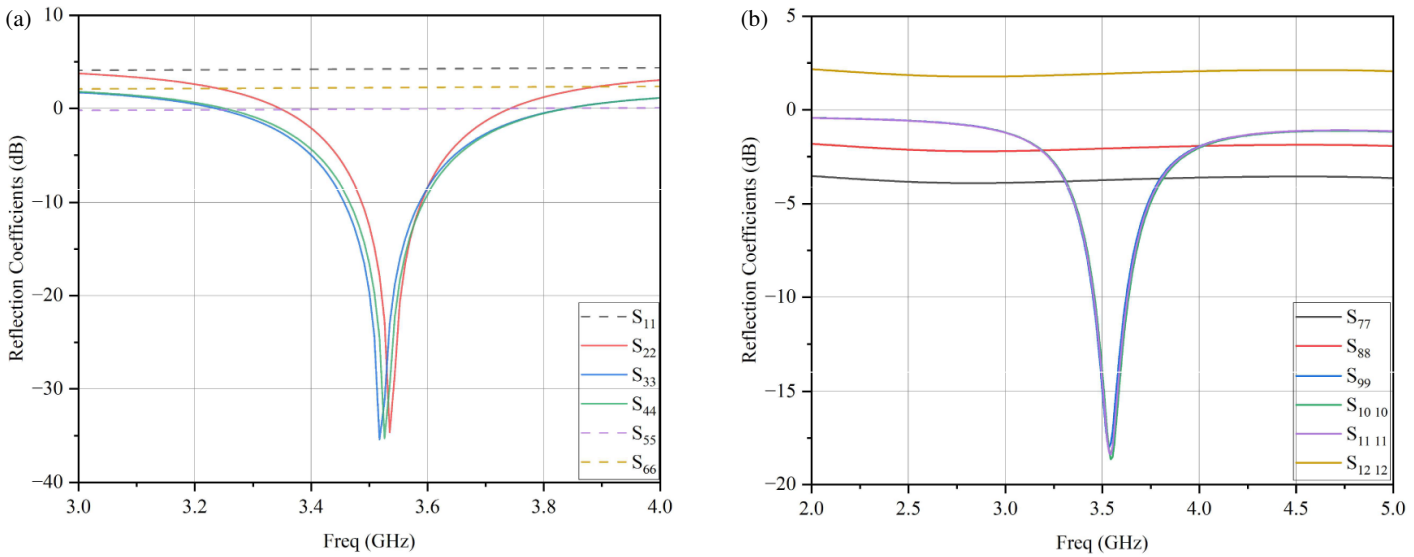


**FIGURE 14**. Simulate reflection Coefficient considering dual hand mode. (a) Ants 1–6. (b) Ants 8–12.

Here, $E_\theta$, $E_\theta j$, $E_\phi i$, and $E_{\phi j}$, are the components of far-field radiation, where $i$ and $j$ are two antenna elements, while $\phi$ and $\theta$ indicate the horizontal and vertical polarizations.

*XPR* is known as the cross polarization ratio between the vertically and horizontal polarized components. The propagation environment's angular power spectrum that satisfies the subsequent conditions is represented by $P_\theta$ and $P_\phi$.

$$\int_0^{2\pi}\int_0^{\pi}(P_\phi)\,d\Omega = 1 \tag{5}$$

$$\int_0^{2\pi}\int_0^{\pi}(P_\theta)\,d\Omega = 1 \tag{6}$$

In simulation it is found that ECC levels are smaller than 0.03 over LTE band 42. These simulated values are less than 0.5 which is the mandatory value for a 5G MIMIO antenna array. Ref. [22] examines the immediate channel capacity of an $M \times M$ MIMO channel H with no transmission medium information on the transmitter section.

$$C = \log_2\left(I_m + \frac{\rho_T}{M}HH^H\right) \tag{7}$$

Here $C$ signifies the capacity of the channel, $I_m$ the unit matrix, and SNR ($\rho_T$) calculated as $\rho_T = \frac{P_T}{\sigma_N^2}P_T$ is the power transmitted while $\sigma_N^2$ is the noise strength on the receiver side. The reference propagation environment used in antenna design is an isolated and uniformly distributed Rayleigh fading channel Hw. The Hw values represent zero-mean circular, balanced

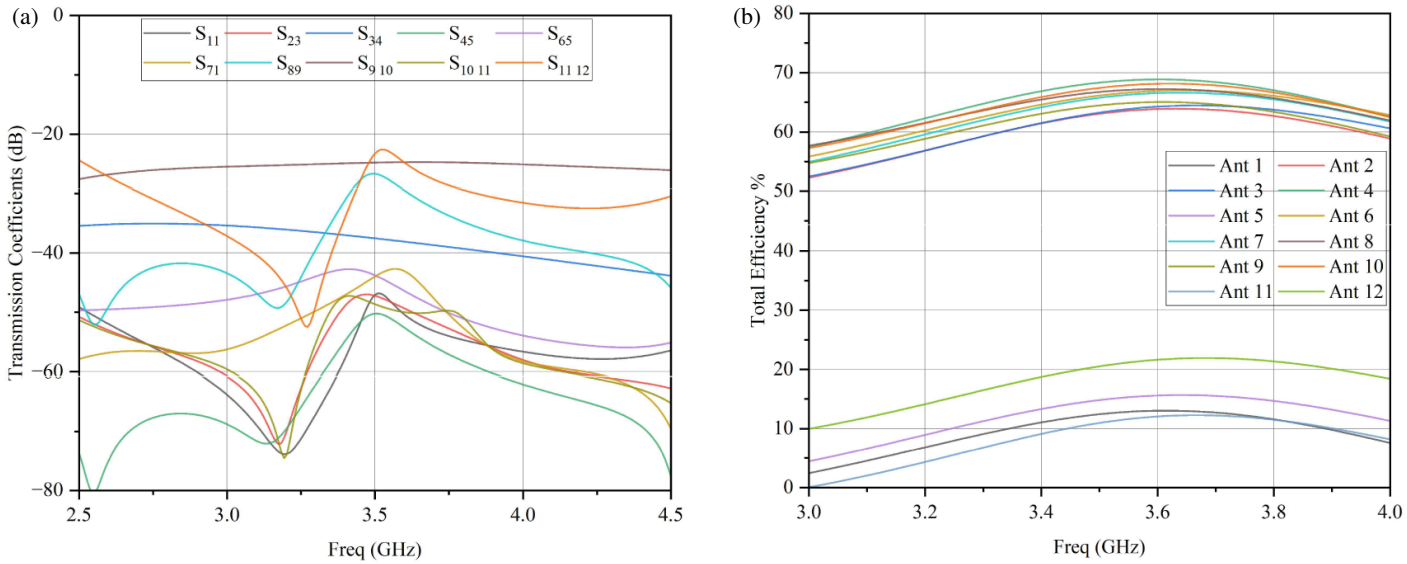


**FIGURE 15**. (a) Transmission coefficient of different antenna elements for dual hand mode. (b) Calculated antenna efficiency for dual hand mode.

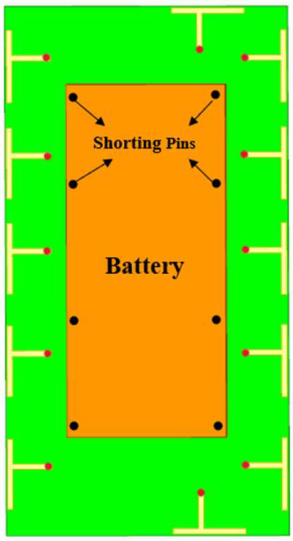


**FIGURE 16**. Simulated model of presented smartphone antenna system with the battery.

Gaussian random variables. For the transmitter radiating element, the MIMO channel is expressed as follows:

$$H = R^{1/2} H_w \tag{8}$$

The gains correlation matrix ($R$) depicts the efficiency, efficiency inequalities, and correlation of receiving antennas. MIMO throughput is commonly quantified using ergodic channel capacity [23], which is calculated by using several Monte Carlo insights of channel matrix $H$. The equation goes as follows:

$$C = E\left(\log_2\left(I_m + \frac{\rho_T}{M} H H^H\right)\right) \tag{9}$$

Figure 10 shows the ergodic channel capacity, using the Kronecker channel mode by mapping 100 000 i.i.d. Rayleigh multipath propagation conditions. The SNR of 20 dB is considered at the receiver, and it is presumed that transmitter has no channel state observations. Ergodic channel capacity of the presented 12 element MIMO array is 65.8 bps/Hz. The upper limit of $12 \times 12$ antenna system is 69 bps/Hz whereas the upper limit of $2 \times 2$ MIMO antenna system is 11.5 bps/Hz.

The diversity gain (DG) is an essential metric for evaluating the effectiveness of the proposed MIMO antenna system. DG is closely related to the envelope correlation coefficient (ECC) and can be estimated using the following standard expression for two-element systems:

$$DG = 10\sqrt{1 - |ECC|^2} \tag{10}$$

Given the very low ECC values ($< 0.03$) observed in our design across the operating band, the corresponding diversity gain approaches the ideal value of 9.99 dB, indicating excellent diversity performance.

### 3.3. User's Hand Impact on MIMO Array

Following section investigates the influence of hand effect on the smartphone. Handheld smartphones are classified into two types, single hand mode (SHM) and dual hand mode (DHM) [24]. Figure 10 depicts two handheld smartphones in SHM and DHM. The impact of the human head has not been studied as huge MIMO systems in the sub-6 GHz region mainly are deployed for data transmission instead of conversational mode.

Figure 11 depicts the connection between antenna ports in SHM, where Ant 11 is in the contact of the hand. In the SHM (Single Hand Mode), it is observed that Antenna 11 comes into contact with the user's finger, leading to a significant degradation in the reflection coefficient. Figure 12 presents the fluctuation in the reflection coefficient with frequency. The other antenna elements show minor variation in their reflection coefficients.

Figure 13(a) shows the effect of user hand SHM on the transmission coefficients of the different antenna elements used in

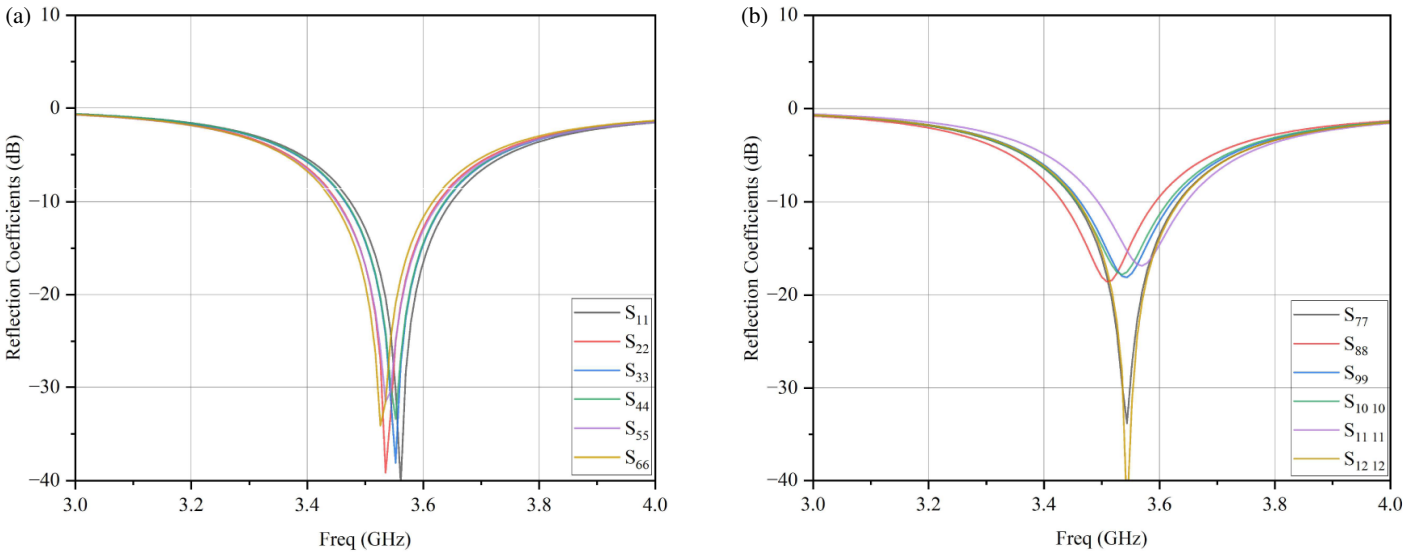


**FIGURE 17**. Reflection coefficients, taking into account the impact of battery. (a) Ants 1–6. (b) Ants 7–12.

**TABLE 1**. Analogy of performance of various arrays of fifth-generation antenna.

| Ref. | Bandwidth (GHz) | ECC/$S_{ij}$ (dB) | Total Efficiency (%) | Antenna size ($\lambda$) | No. of elements | Channel Capacity (bps/Hz) |
|---|---|---|---|---|---|---|
| Presented | 3.4–3.6 ($-10$ dB) | $0.03/ < -20$ | 66–76 | $0.239\lambda \times 0.052\lambda$ | $(12 \times 12)$ | 65.8 |
| [13] | 3.4–3.6 ($-10$ dB) | $0.2/ < -10$ | 40–60 | $0.08\lambda \times 0.12\lambda$ | $(8 \times 8)$ | 36 |
| [15] | 3.4–3.6 ($-10$ dB) | $0.012/ < -19.1$ | 59–68 | $0.19\lambda \times 0.06\lambda$ | $(8 \times 8)$ | Not given |
| [16] | 3.4–3.6 ($-6$ dB) | $0.07/ < -17$ | 49–61 | $0.13\lambda \times 0.08\lambda$ | $(8 \times 8)$ | Not given |
| [19] | 3.4–3.8 ($-10$ dB) | $0.1/ < -10$ | 42–62 | $0.036\lambda \times 0.096\lambda$ | $(10 \times 10)$ | 47 |
| [25] | 3.4–3.6 ($-10$ dB) | $0.1/ < -17$ | $> 58$ | $0.16\lambda \times 0.03\lambda$ | $(4 \times 4)$ | 19 |
| [26] | 3.4–3.6 ($-6$ dB) | $0.13/ < -12.7$ | 39–50 | $0.173\lambda \times 0.035\lambda$ | $(4 \times 4)$ | Not given |
| [27] | 3.4–3.6 ($-6$ dB) | $0.32/ < -10$ | 40–60 | $0.035\lambda \times 0.58\lambda$ | $(16 \times 16)$ | 70 |
| [28] | 3.4–3.6 ($-10$ dB) | $0.05/ < -17.5$ | 62–76 | $0.035\lambda \times 0.25\lambda$ | $(8 \times 8)$ | 40.8 $(8 \times 8)$ |

the MIMO configuration. Some deflections are observed in the results for the transmission coefficients. In Figure 13(b), the efficiencies are shown considering the effect of user hand in single hand mode (SHM).

It is clearly seen that due to the hand grip there is deflection in the total efficiencies for the single hand mode. The total efficiency of Ant 11 goes below 15%, and there is also a decrease in the total efficiency of the Ant 12 which goes below 52%. Also, there is decrease in the isolation of the antenna components greater than $-23$ dB which is still good. The same impact is observed for the dual hand mode when the parameters are simulated. In DHM, Ants 1, 5, 6, 7, 8, and 12 are blocked due to the orientation of hand to hold the smartphone.

Figure 14 displays the reflection coefficients for antenna components in DHM. Ants 1, 5, 6, 7, 8, and 12 are in initial contact with operator's hands, resulting in changed reflection coefficients.

Figure 15 illustrates the transmission coefficients between different pairs of antenna elements. In Dual Hand Mode (DHM), changes in the isolation levels among the antenna elements are observed; however, the isolation remains above 18 dB. A change in total efficiencies is also observed in DHM, where the efficiency of antenna elements in contact with the hand drops below 20%, as shown in Figure 15(b).

### 3.4. Smartphone Battery Impact

To find out the actual effectiveness of the designed architecture, we introduced a metallic block resembling a typical smartphone battery, measuring 102 mm $\times$ 47 mm $\times$ 5 mm. This block was positioned on the top layer of the PCB and grounded using eight electrically conducting shorting pins, as shown in Figure 16. Despite its proximity to the antenna elements, the battery module had minimal effect on radiation performance, demonstrating the robustness of the antenna design. Simulated results in Figure 17 indicate that the reflection coefficients remain more than 10 dB across the operational frequency range, confirming that impedance matching is maintained even with the battery in place. Figure 18 shows the transmission coefficients between antenna elements, where the isolation remains better than 18 dB. Although there is a slight reduction in isolation, the overall MIMO performance remains within acceptable limits, making the antenna suitable for practical 5G smartphone solutions.

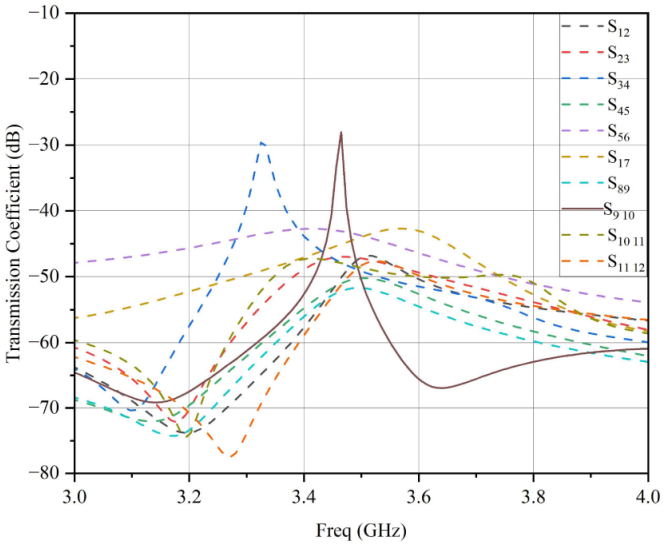


**FIGURE 18**. Transmission coefficients of different antenna elements considering the impact of battery.

The performance comparison in Table 1 highlights the proposed antenna's clear advantage over existing designs.

## 4. CONCLUSION

This study describes a 12-element MIMO antenna using slotted antennas that feature open decoupling slots. The presented MIMO antenna system has a $-10$ dB bandwidth of roughly 900 MHz, encompassing the LTE 42 frequency band. The antenna's simple design avoids the need for external decoupling systems, making it easier to manufacture. The proposed architecture delivers exceptional achievement using MIMO parameters such as low mutual coupling ($-20$ dB), passable ECC ($< 0.03$), and entire efficiency $> 66\%$. The proposed $12 \times 12$ MIMO antenna formation (with SNR equals 20 dB) outperforms a $2 \times 2$ MIMO system in terms of peak ergodic channel capacity by 65.8%. The presented composition is appropriate for future 5G devices.

## REFERENCES

[1] Hong, W., "Solving the 5G mobile antenna puzzle: Assessing future directions for the 5G mobile antenna paradigm shift," *IEEE Microwave Magazine*, Vol. 18, No. 7, 86–102, Nov.–Dec. 2017.

[2] Li, Y., Y. Luo, G. Yang, *et al.*, "12-port 5G massive MIMO antenna array in sub-6 GHz mobile handset for LTE bands 42/43/46 applications," *IEEE Access*, Vol. 6, 344–354, 2017.

[3] Xu, H., H. Wang, S. Gao, H. Zhou, Y. Huang, Q. Xu, and Y. Cheng, "A compact and low-profile loop antenna with six resonant modes for LTE smartphone," *IEEE Transactions on Antennas and Propagation*, Vol. 64, No. 9, 3743–3751, Sep. 2016.

[4] Zhang, S., Z. Ying, J. Xiong, and S. He, "Ultrawideband MIMO/diversity antennas with a tree-like structure to enhance wideband isolation," *IEEE Antennas and Wireless Propagation Letters*, Vol. 8, 1279–1282, 2009.

[5] Lee, J.-Y., S.-H. Kim, and J.-H. Jang, "Reduction of mutual coupling in planar multiple antenna by using 1-D EBG and SRR structures," *IEEE Transactions on Antennas and Propagation*, Vol. 63, No. 9, 4194–4198, Sep. 2015.

[6] Li, Z., Z. Du, M. Takahashi, K. Saito, and K. Ito, "Reducing mutual coupling of MIMO antennas with parasitic elements for mobile terminals," *IEEE Transactions on Antennas and Propagation*, Vol. 60, No. 2, 473–481, Feb. 2012.

[7] Zhang, S., B. K. Lau, Y. Tan, Z. Ying, and S. He, "Mutual coupling reduction of two PIFAs with a T-shape slot impedance transformer for MIMO mobile terminals," *IEEE Transactions on Antennas and Propagation*, Vol. 60, No. 3, 1521–1531, Mar. 2012.

[8] Ban, Y.-L., C. Li, G. Wu, K.-L. Wong, and e. al., "4G/5G multiple antennas for future multi-mode smartphone applications," *IEEE Access*, Vol. 4, 2981–2988, 2016.

[9] Alibakhshikenari, M., F. Babaeian, B. S. Virdee, S. Aïssa, L. Azpilicueta, C. H. See, A. A. Althuwayb, I. Huynen, R. A. Abd-Alhameed, F. Falcone, and E. Limiti, "A comprehensive survey on "Various decoupling mechanisms with focus on metamaterial and metasurface principles applicable to SAR and MIMO antenna systems"," *IEEE Access*, Vol. 8, 192 965–193 004, 2020.

[10] Alibakhshikenari, M., B. S. Virdee, and E. Limiti, "Study on isolation and radiation behaviours of a 34×34 array-antennas based on SIW and metasurface properties for applications in terahertz band over 125-300 GHz," *Optik*, Vol. 206, 163222, Mar. 2020.

[11] Alibakhshikenari, M., B. S. Virdee, P. Shukla, C. H. See, R. A. Abd-Alhameed, F. Falcone, K. Quazzane, and E. Limiti, "Isolation enhancement of densely packed array antennas with periodic MTM-photonic bandgap for SAR and MIMO systems," *IET Microwaves, Antennas & Propagation*, Vol. 14, No. 3, 183–188, 2019.

[12] Alibakhshikenari, M., M. Khalily, B. S. Virdee, C. H. See, R. A. Abd-Alhameed, and E. Limiti, "Mutual-coupling isolation using embedded metamaterial EM bandgap decoupling slab for densely packed array antennas," *IEEE Access*, Vol. 7, 51 827–51 840, 2019.

[13] Wong, K.-L., C.-Y. Tsai, and J.-Y. Lu, "Two asymmetrically mirrored gap-coupled loop antennas as a compact building block for eight-antenna MIMO array in the future smartphone," *IEEE Transactions on Antennas and Propagation*, Vol. 65, No. 4, 1765–1778, Apr. 2017.

[14] Wong, K.-L., B.-W. Lin, and B. Li, "Dual-band dual inverted-F/loop antennas as a compact decoupled building block for forming eight 3.5/5.8-GHz MIMO antennas in the future smartphone," *Microwave and Optical Technology Letters*, Vol. 59, No. 11, 2715–2721, 2017.

[15] Zhao, A. and Z. Ren, "Size reduction of self-isolated MIMO antenna system for 5G mobile phone applications," *IEEE Antennas and Wireless Propagation Letters*, Vol. 18, No. 1, 152–156, Jan. 2019.

[16] Sun, L., H. Feng, Y. Li, and Z. Zhang, "Compact 5G MIMO mobile phone antennas with tightly arranged orthogonal-mode pairs," *IEEE Transactions on Antennas and Propagation*, Vol. 66, No. 11, 6364–6369, Nov. 2018.

[17] Ling, X. and R. Li, "A novel dual-band MIMO antenna array with low mutual coupling for portable wireless devices," *IEEE Antennas and Wireless Propagation Letters*, Vol. 10, 1039–1042, 2011.

[18] Al-Hadi, A. A., J. Ilvonen, R. Valkonen, and V. Viikari, "Eight-element antenna array for diversity and MIMO mobile terminal in LTE 3500 MHz band," *Microwave and Optical Technology Letters*, Vol. 56, No. 6, 1323–1327, 2014.

[19] Wong, K.-L. and J.-Y. Lu, "3.6-GHz 10-antenna array for MIMO operation in the smartphone," *Microwave and Optical Technology Letters*, Vol. 57, No. 7, 1699–1704, 2015.

[20] Li, M.-Y., Y.-L. Ban, Z.-Q. Xu, G. Wu, C.-Y.-D. Sim, K. Kang, and Z.-F. Yu, "Eight-port orthogonally dual-polarized antenna array for 5G smartphone applications," *IEEE Transactions on Antennas and Propagation*, Vol. 64, No. 9, 3820–3830, Sep. 2016.

[21] Zhang, Z., *Antenna Design for Mobile Devices*, John Wiley & Sons, 2017.

[22] Sharawi, M. S., A. T. Hassan, and M. U. Khan, "Correlation coefficient calculations for MIMO antenna systems: A comparative study," *International Journal of Microwave and Wireless Technologies*, Vol. 9, No. 10, 1991–2004, 2017.

[23] Tian, R., B. K. Lau, and Z. Ying, "Multiplexing efficiency of MIMO antennas," *IEEE Antennas and Wireless Propagation Letters*, Vol. 10, 183–186, 2011.

[24] Zhang, S., K. Zhao, Z. Ying, and S. He, "Adaptive quad-element multi-wideband antenna array for user-effective LTE MIMO mobile terminals," *IEEE Transactions on Antennas and Propagation*, Vol. 61, No. 8, 4275–4283, Aug. 2013.

[25] Ren, Z., A. Zhao, and S. Wu, "Mimo antenna with compact decoupled antenna pairs for 5G mobile terminals," *IEEE Antennas and Wireless Propagation Letters*, Vol. 18, No. 7, 1367–1371, Jul. 2019.

[26] Chang, L., Y. Yu, K. Wei, and H. Wang, "Polarization-orthogonal co-frequency dual antenna pair suitable for 5G MIMO smartphone with metallic bezels," *IEEE Transactions on Antennas and Propagation*, Vol. 67, No. 8, 5212–5220, Aug. 2019.

[27] Wong, K.-L., J.-Y. Lu, L.-Y. Chen, W.-Y. Li, and Y.-L. Ban, "8-antenna and 16-antenna arrays using the quad-antenna linear array as a building block for the 3.5-GHz LTE MIMO operation in the smartphone," *Microwave and Optical Technology Letters*, Vol. 58, No. 1, 174–181, Jan. 2016.

[28] Li, Y., Y. Luo, G. Yang, and e. al., "High-isolation 3.5 GHz eight-antenna MIMO array using balanced open-slot antenna element for 5G smartphones," *IEEE Transactions on Antennas and Propagation*, Vol. 67, No. 6, 3820–3830, Jun. 2019.